Heliyon 10 (2024) e33674

Contents lists available at ScienceDirect

Heliyon

journal homepage: www.cell.com/heliyon

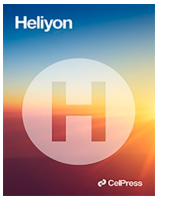

Research article

Induction of ferroptosis by brucine suppresses gastric cancer progression through the p53-mediated SLCA711/ALOX12 axis

Jincheng Zhai *, Jiaxing Min, Mingqiang Gong

Department of Critical Care Medicine, Fengxin County People Hospital, Yichun, 330700, Jiangxi, PR China

ARTICLE INFO

Keywords:
Brucine
Ferroptosis
Gastric cancer
p53
SLCA711/ALOX12

ABSTRACT

Increasing evidence indicates important antiproliferative and anti-inflammatory roles of brucine in various diseases. However, the mechanism through which brucine causes the cell death of gastric cancer (GC) remains unclear. In the current research, we looked into whether brucine inhibits GC progression. GC cell migration and proliferation were assessed in response to brucine using Transwell, scratch, and the Cell Counting Kit-8 (CCK-8) assays. To assess the expression of proteins linked to ferroptosis, western blotting was used. An in vivo experiment was conducted to investigate if brucine decreases tumor growth. The CCK-8 experiment demonstrated that brucine reduced AGS and MKN45 cell viability in a way that was dose- and time-dependent. Brucine dramatically promoted cell death in AGS and MKN45 cells according to flow cytometry. In addition, brucine reduced AGS and MKN45 cells' ability to migrate. According to Western blot investigations, brucine elevated p53 and ALOX12 expression, while suppressing the expression of SLC7A11 in AGS and MKN45 cells. Notably, silencing p53 reversed brucine-induced ferroptotic cell death. Additionally, brucine was shown to decrease tumor weight and volume in in vivo experiments. Moreover, malondialdehyde (MDA) and Fe2+ levels decreased in response to brucine treatment. Furthermore, in tumors treated with brucine, p53 and ALOX12 expression increased, whereas SLCA711 expression decreased. In summary, we demonstrated that brucine regulates the p53/SLCA711/ALOX12 axis to cause ferroptosis in GC cells. The results of this study lend support to the idea of treating GC with brucine.

1. Introduction

Globally, gastric cancer (GC) ranks third in terms of cause of death and is the fifth most frequent type of cancer [1]. The main danger signs for GC include gastroesophageal reflux disease, *Helicobacter pylori* infection, poor eating habits, and obesity [2]. Despite major advancements in treatment approaches over the years, the median survival time for GC remains low because to high occurrences of metastasis and recurrence, as well as limited response to radiation and chemotherapy [3,4]. Thus, more research into the root cause molecules and the development of novel chemotherapeutic drugs are needed to enhance the outcome of GC patients.

A recently discovered kind of cell death named ferroptosis is brought on by a buildup of iron, elevated lipid reactive oxygen species (ROS) and malondialdehyde (MDA) levels, and decreased glutathione (GSH) levels [5,6]. Via the cystine/glutamate transporter system (system Xc-, via SLC7A11 and SLC3A2), cells absorb cystine from the extracellular milieu. Cysteine is necessary for the internal synthesis of the reducing agent glutathione (GSH) [7]. Glutathione peroxidase 4 (GPX4) converts peroxidized lipids into harmless

* Corresponding author.
E-mail address: xueguanke0898@163.com (J. Zhai).

https://doi.org/10.1016/j.heliyon.2024.e33674
Received 24 August 2023; Received in revised form 24 June 2024; Accepted 25 June 2024
Available online 26 June 2024

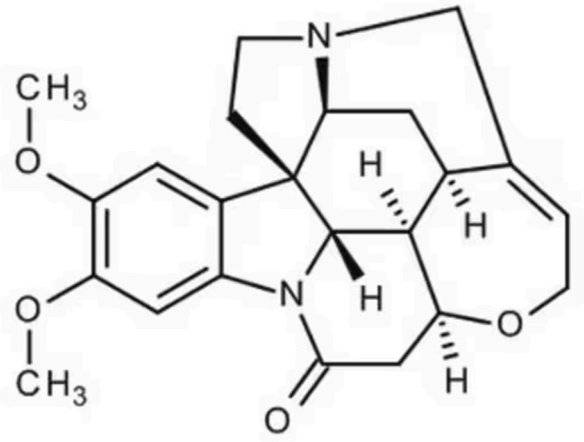

Fig. 1. The structure of brucine.

lipols using GSH supplementation; this process is a critical cell protection mechanism versus ferroptosis [7]. A significant part of GPX4-induced ferroptosis inhibition is played by ACSL4. ACSL4 integrates polyunsaturated fatty acids (PUFAs) into phospholipids, which are the primary source of lipid peroxidation; thus, cells deficient in ACSL4 resist GPX4 inhibition-induced ferroptosis [8,9]. Jiang et al. first reported that p53 might cause ferroptosis in malignant cells through the transcriptional repression of SLC7A11 [10]. In another study, p53-regulated ferroptosis was shown to be dependent on arachidonate 12-lipoxygenase and 12S type (ALOX12) expression, but not on the GPX4-ACSL4 axis [11]. Mechanistically, SLC7A11 interacts with ALOX12, and this interaction inhibits the lipoxygenase activity of ALOX12, which attenuates the peroxidation of PUFA-containing phospholipids, ultimately antagonizing ferroptosis and promoting tumor progression [11].

Brucine, a weakly alkaline indole alkaloid (Fig. 1), is an active ingredient in the seeds of Strychnos nux-vomica and belongs to the Loganiaceae family [12]. Increasing evidence indicates important antiproliferative and antiseptic properties of brucine in various diseases [13,14]. In one instance, brucine causes cervical cancer cells to undergo apoptosis by modulating PI3K/AKT/mTOR signaling [13]. Brucine also promotes immunogenic cell death by impairing autophagy [14]. A recent report indicated that brucine induces ferroptosis in glioma [15]. However, whether brucine contributes to GC cell death is still being elucidated.

In this work, we explored the role of brucine in GC progression, both in vitro and in vivo. Analyzing the biological process by which brucine has its anti-GC impact was the goal of this investigation. This offers a theoretical foundation for its practical application of brucine in GC treatment and expand our understanding of the antitumor molecular mechanisms of brucine.

2. Materials and methods

2.1. Cell culture

MKN45 and AGS cells harboring wild-type p53 were purchased from Procell (Wuhan, China). The GES-1 (human gastric mucosal) cell line was purchased from SUNNCELL (Wuhan, China). Short-tandem repeat (STR) profiling was used for cell authentication. MKN45 cells were grown in Roswell Park Memorial Institute (RPMI)-1640 medium (GE Healthcare, Logan, USA), and AGS cells were grown in Ham's F-12 medium (GE Healthcare) in a six well plate (Corning, USA). At 37 °C in an incubator (Labtrip, Nanjing, China) with 5 % CO2, each culture media had been added with 0.1 mg/mL streptomycin (GE Healthcare), 100 units/mL penicillin (GE Healthcare), and 10 % fetal bovine serum (FBS; Gibco, USA).

2.2. Cell proliferation assay

To investigate the impact of brucine on MKN45 and AGS cell viability, a Cell Counting Kit-8 (CCK-8) test was conducted. AGS and MKN45 cells' viabilities were assessed via a CCK-8 assay kit (Sorabio, Beijing, China). In summary, 3000 cells per well of MKN45 and AGS cells were sown in 96-well plates for a duration of 24 h. Next, the MKN45 and AGS cells were incubated with brucine (5892-11-5, purity: 98 %, Mainchem Co.,. Xiamen, China) at a density of 0, 3.125, 6.25, 12.5, 25, 50, or 100 μM and 0, 0.5, 1, 5, 10, 20, or 30 μM for 24 h at 37 °C. Next, a Bio-Tek EL 800 plate reader was used to measure the cell viability at 450 nm after adding 10 μL of CCK-8 solution to each well for 4 h at 37 °C (Minneapolis, USA).

To investigate what kind of cellular death can be caused by brucine, AGS and MKN45 cells were preincubated with a pancaspase inhibitor (z-VAD-FMK, 20 μM; MCE, Monmouth Junction, USA), necrosis inhibitor (necrostatin-1 [Nec-1], 20 μM; MCE), ferroptosis inhibitor (ferrostatin-1 [Fer-1, 1 μM, MCE), or autophagy inhibitor (3-methyladenine [3-MA], 20 μM; MCE) for 1 h at 37 °C. Thereafter, 15 or 10 μM brucine was applied to the AGS and MKN45 cells for a full day at 37 °C. The CCK-8 solution was used to assess cell viability, as described above. The percentage of dead cells (%) were quantified as follows:

Dead cells (%) = (1.000-OD experimental group)/OD control group × 100

2.3. Characterization of MDA, glutathione (GSH), and Fe^{2+} concentrations

To validate the role of brucine in ferroptosis, MDA, GSH, and Fe2+ levels were determined. After being planted at a density of 5 × 105 cells/well in six-well plates, AGS and MKN45 cells were incubated for the whole night. 10 μM N-acetyl-L-cysteine (NAC, S0077; Beyotime Biotechnology, Shanghai, China) was added to the cells and incubated them for 1 h at 37 °C. Thereafter, the cells underwent a 24 h treatment at 37 °C with either 15 or 10 μM brucine. The cells were collected and the intracellular MDA, GSH, and Fe2+ levels were quantified using a Lipid Peroxidation MDA Assay Kit (S0131; Beyotime Biotechnology), GSH assay kit (BC1175; Solarbio), and iron assay kit (ab83366; Abcam, Cambridge, UK) according to the manufacturer's instructions [16–18].

2.4. Glutathione peroxidase assay

Following the instructions provided by the manufacturer, a Glutathione Peroxidase Assay Kit (colorimetric, ab102530; Abcam) was used to assess the impact of brucine on the glutathione peroxidase activity [19]. 340 nm was the absorbance obtained with a Bio-Tek EL 800 plate reader (Bio-Tek).

2.5. Flow cytometry assay

Using flow cytometry, the implications of brucine on cell death were investigated. An assay kit called Annexin V-FITC/7-AAD (P-CA-202; Procell) was used to quantify cells that were dead. After being seeded at an average density of 5 × 105 cells/well in six-well plates, AGS and MKN45 cells were incubated for a whole night at 37 °C. Thereafter, the cells underwent a 24 h treatment at 37 °C with either 15 or 10 μM brucine. After that, the cells were dyed for 10 min at room temperature in the dark using 5 μL of Annexin V-APC and 5 μL of 7-AAD. An BD FACSCantoII flow cytometer (BD Biosciences, Franklin Lakes, USA) was used to quantify cells that were dead, and FlowJo software was used to analyze the data (Shanghai, China). Whereas Q3 reflects early apoptotic cells, Q2 symbolizes necrotic and late apoptotic cells. Thus, in this investigation, only cells in the Q2 region were taken into account.

2.6. Cell migration assays

Using a Transwell experiment, the effects of brucine on AGS and MKN45 cell migration were investigated. AGS and MKN45 cells were planted at a density of 105 cells/well in the upper chambers of a Transwell plate (Corning) and left overnight at 37 °C for migration tests. To the lower chambers, fresh medium with 20 % FBS was introduced. After that, the cells underwent a 24 h treatment at 37 °C with either 15 or 10 μM brucine. The migratory cells that pierced the membrane's lower surface were preserved for 20 min at room temperature in 4 % paraformaldehyde (Beyotime Biotechnology) and stained for 20 min at room temperature in 0.1 % crystal violet (Solarbio). A light microscope was used for observing the cells in five randomly chosen visual fields (CX31; Olympus Corporation, Tokyo, Japan).

AGS and MKN45 cells were planted in six-well plates at a cell count of 5 × 105 cells/well for the scratch test, and they were left overnight at 37 °C. Next, the cells were incubated with 1 % FBS RPMI-1640 and F12 medium and treated with 15 or 10 μM brucine or vehicle for 24 h at 37 °C. A scratch test was performed with 1 % FBS in the cell culture medium because the use of a low-serum medium reduced the effect of cell proliferation on the experimental results. Photographs of the wounds were taken with a white-light microscope (CX31; Olympus Corporation) at 0 and 24 h. Using ImageJ 1.43b software (National Institutes of Health, Bethesda, USA), the dimensions of the scratch was examined. (Initial wound area - Current wound area)/Initial wound area × 100 % was the formula used to determine the wound healing rate.

2.7. Cell invasion assay

After allowing Matrigel (BD Biosciences) to naturally melt at 4 °C for the entire night, and 500 μL of Matrigel + 500 μL of RPMI-1640 was gently mixed. After drying for 4 h at 37 °C, 70 μL of the mixture was then applied to the upper chamber of a 24-well plate. Thereafter, 100 μL (5×10^4) of cells were digested and resuspended in the upper chamber at 37 °C. 100 μL (5×10^4) of the cells were transferred to the upper chamber (serum-free media) after 24 h at 37 °C, and the lower chamber was incubated with RPMI-1640 culture with 10 % FBS for 24 h at 37 °C. For 20 min at room temperature, the cells were treated alongside 0.1 % crystal violet (Solarbio). The upper cell layer of the Transwell plate was removed, and the membrane was removed from the bottom. By applying a light microscope, five visual regions were arbitrarily chosen for the purpose to count the cells (CX31; Olympus Corporation).

2.8. Transient transfection

To further explore whether brucine induces ferroptosis through p53, a specific siRNA targeting p53 was used. p53 siRNA (5′-ACUGUUACACAUGUAGUUGUA-3′) and scrambled negative control (NC, 5′-CCGAUAGGUUUACUGCCAATT-3′) were acquired

through GenePharma (Shanghai, China). With the HiperFect transfection reagent, the siRNAs were transfected into AGS and MKN45 cells (Qiagen, Duesseldorf, Germany). To summarize, 100 μL of serum-free F-12 medium was heated to 37 °C and treated with 10 μM 2 μL of siRNA. After that, 2 μL of Qiagen's HiperFect transfection reagent was incorporated, and the mixture underwent incubation for 10 min at 37 °C at room temperature. Subsequently, the mixture was poured to each well of a six-well plate containing 104 μL, and the cells were cultured for 24 h at 37 °C before undergoing additional examination.

2.9. Immunofluorescence (IF) staining

The implications of brucine on p53 expression were assessed by IF. AGS and MKN45 cells were blocked for 20 min at ambient temperature in 4 % paraformaldehyde (Beyotime Biotechnology). The cells were subsequently incubated for 2 h at room temperature with 5 % bovine serum albumin (BSA, Sigma-Aldrich, St. Louis, USA) after being permeabilized for 20 min with 0.5 % Triton X-100. The cells were incubated with a primary antibody against p53 (1:100, 2527, Cell Signaling Technology, Inc., Danvers, USA) at 4 °C for an overnight period after three rounds of washing in phosphate-buffered saline with 0.1 % Tween (PBST). After that, the cells underwent treatment for 2 h at room temperature and in the dark with a goat anti-rabbit secondary antibody conjugated with TRITC (1:50, ZF-0317, Beijing Zhongshan Golden Bridge Biotechnology Co., Beijing, China). A fluorescent microscope (BX63, Olympus Corporation) was used to take representative pictures.

2.10. Quantification of lipid peroxidation

The buildup of lipid-derived ROS is a marker of ferroptosis. Therefore, we quantified lipid peroxidation in brucine-treated AGS and MKN45 cells. After being planted at an amount of 5 × 105 cells/well in six-well plates, AGS and MKN45 cells were incubated for the whole night. 10 μM N-acetyl-L-cysteine (NAC, S0077, Beyotime Biotechnology) was added to the cells and incubated them for 1 h at 37 °C. After that, the cells were incubated at 37 °C for 24 h at 15 or 10 μM brucine. With a C11 BODIPY fluorescent probe (HY-D1301, MCE) in accordance with the producer's instructions, intracellular lipid peroxidation was measured. In summary, the cells underwent treatment for 20 min at 37 °C in the dark using 5 μM C11 BODIPY fluorescent probe. Thereafter, the cells were rinsed at room temperature for 5 min each time using fresh culture media devoid of FBS for three times. Intracellular lipid peroxidation was investigated using a fluorescence microscope (BX63, Olympus Corporation). For the quantitative analysis of fluorescence signals, we used the ImageJ 1.43b software (National Institutes of Health, Bethesda, USA) to apply thresholding to fluorescence images, enabling the segmentation of fluorescence signals and background regions. This approach facilitates the extraction of individual fluorescence signal intensities for subsequent statistical analyses.

2.11. Transmission electron microscopy (TEM)

To see alterations in the mitochondria's ultrastructure, TEM examination was carried out. The cells were first post-fixed in 2 % osmium tetroxide and 1.5 % potassium ferrocyanide for 1 h at room temperature after being fixed in 2.5 % glutaraldehyde solution (Zhongxingbairui Co., Beijing, China) for an overnight period at 4 °C. The samples then underwent dehydration in various grades of ethanol (30–100 %) and acetone solutions, rinsed in water, and contrasted en bloc with uranyl acetate (Zhongxingbairui Co.). The anhydrous acetone (Zhongxingbairui Co.) and epoxy resin (Zhongxingbairui Co.) gradient infiltration method was used to prepare the samples. The samples were then immersed in resin (Zhongxingbairui Co.) and polymerized for 48 h at 60 °C. A Reichert Ultracut S ultramicrotome (Science Service, Munich, Germany) was used to cut ultrathin sections, which were then contrasted with lead citrate. With an EM 10 CR electron microscope (Carl Zeiss, Jena, Germany), pictures were taken.

2.12. Western blot analysis

Tumor tissues and AGS and MKN45 cells were used to isolate total protein via the radioimmunoprecipitation assay (RIPA) buffer (Solarbio). The protein concentration was ascertained by a bicinchoninic acid (BCA) test kit (Pierce; Thermo Fisher Scientific, Inc., Waltham, USA) following centrifugation at 13,000×*g* for 20 min at 4 °C. Following 12 % sodium dodecyl-sulfate polyacrylamide gel electrophoresis (SDS-PAGE), 20 μg of identical protein were loaded onto polyvinylidene fluoride (PVDF) membranes (Millipore, Billerica, USA). The membranes were blocked for 2 h at room temperature using 5 % skim milk (Thermo Fisher Scientific, Inc.). Afterwards, the membranes were treated with the primary antibodies listed below: anti-p-p53 (9284; 1:1000, CST), anti-p53 (9282; 1:1000; CST), anti-ALOX12 (ab168384, 1:1000; Abcam), anti-GPX4 (ab252833, 1:1000; Abcam), anti-SLC7A11 (ab307601, 1:1000; Abcam), and β-actin (4970, 1:3000; CST) at 4 °C overnight. The membranes were then incubated for 2 h at room temperature with goat anti-rabbit IgG conjugated with horseradish peroxidase (HRP) (1:5000; cat. no. ZB-2301; Beijing Zhongshan Golden Bridge Biotechnology Co.). Enhanced chemiluminescence (ECL; EMD Millipore) was utilized to detect protein bands, and densitometric analyses were performed using ImageJ 1.43b software (National Institutes of Health, Bethesda, MD, USA). An internal control was employed, namely β-Actin.

2.13. Examining the tumorigenicity of nude mice

We bought twenty male BALB/c nude mice from SPF (Beijing) Biotechnology Co., Ltd. (Beijing, China) at an average age of eight weeks and a mass of 20.41 ± 1.20 g. Every mouse was kept in a pathogen-free environment with an ad libitum supply of food and water

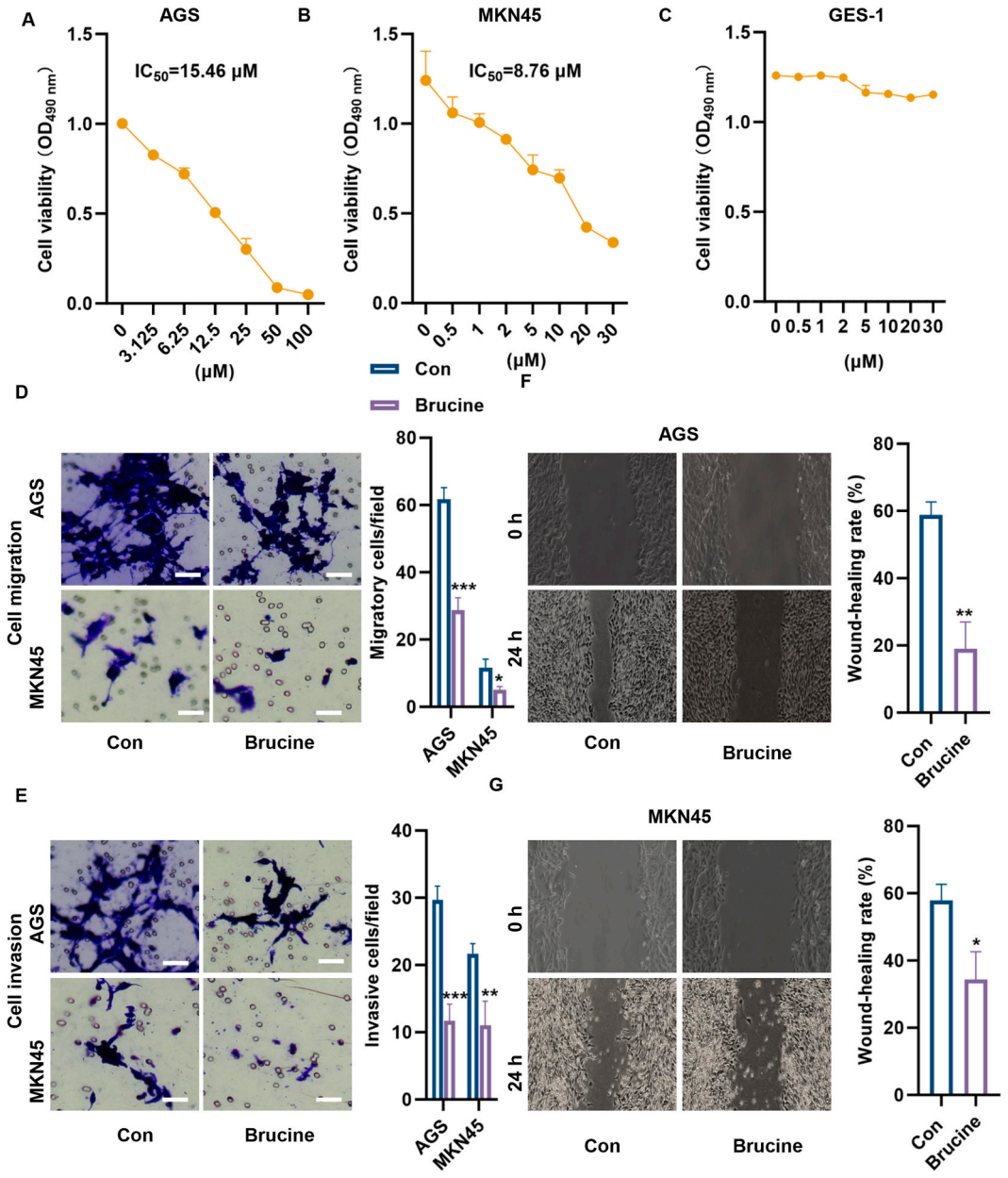

Fig. 2. Brucine suppressed GC cell proliferation and migration. The CCK-8 assay showed that brucine decreased AGS (A), MKN45 (B), and GES-1 (C) cell viability in a dose-dependent manner. Transwell assays showed that, compared with the control treatment, brucine treatment significantly suppressed AGS and MKN45 cell migration (D) and invasion (E) (magnification, 20 × ; scale bar, 20 μm). Scratch test analysis also revealed that, compared with the control treatment, brucine treatment decreased the wound healing rate of AGS (F) and MKN45 (G) cells (magnification, 20 × ; scale bar, 10 μm). n = three independent replicates for each individual experiment. **p < 0.01, ***p < 0.001 vs. con.

in a regular 12 h light-dark cycle at 25 °C. The mice (n = 10) were subcutaneously administered with 100 μL of normal saline containing around 4 × 106 MKN45 cells in their right flanks. All mice were divided into two groups, with five mice in each: (1) control group and (2) 3 mg/kg brucine group. The mice received tail vein injections once a day for 28 days of either brucine or regular saline. Animal health and behavior were monitored daily. Throughout the trial, no mice perished. A tumor's maximum diameter of more than 2 cm was deemed the study's humane endpoint. Four weeks later, under profound isoflurane anesthesia (5 %), all surviving mice were decapitated to end their lives [20]. The following were markers of the level of anesthesia: the corneal reflex vanished, the deep, slow, and steady breathing became deeper, the muscles of the head, neck, and limbs relaxed, and the skin pinching reaction vanished. Death was confirmed by checking for the lack of heartbeat and pupillary responses to light and respiration. The tumors were then gathered, and the primary tumor mass was determined. The formula used to calculate the tumor volume was volume = (length × width^2)/2.

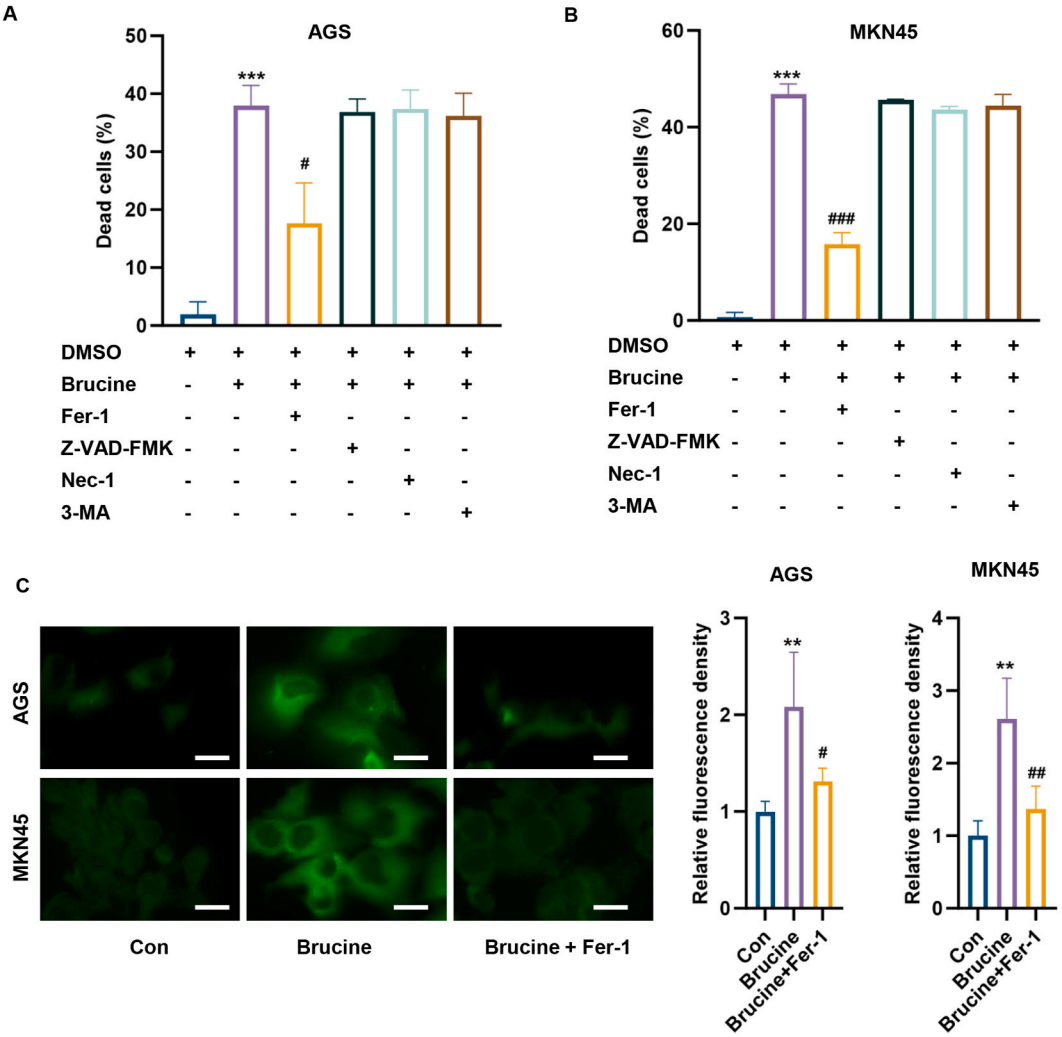

Fig. 3. Brucine induced ferroptosis in GC cells. AGS and MKN45 cells were preincubated with a pancaspase inhibitor (z-VAD-FMK, 20 μM), a necrosis inhibitor (Ner-1, 20 μM), a ferroptosis inhibitor (Fer-1, 1 μM), or an autophagy inhibitor (3-MA, 10 μM) for 2 h and then treated with 15 or 10 μM brucine for 24 h. Fer-1 significantly protected GC cells from brucine-induced cell death compared to control AGS (A) and MKN45 (B) cells. (C) A C11 BODIPY fluorescent probe was used to detect the fluorescence intensity in AGS and MKN45 cells exposed to brucine (magnification, 20 × ; scale bar, 10 μm). n = three independent replicates for each individual experiment. ***p < 0.001 vs. con; ##p < 0.01, ###p < 0.001 vs. brucine.

The Fengxin County People's Hospital's Animal Ethics Committee approved experimental protocols and animal care (20231252).

2.14. Statistical analysis

GraphPad Prism 7 (GraphPad Software Co., Version X, USA) was used for the statistical analysis, and all the data are presented as mean ± standard deviation (SD). An unpaired Student's two-tailed *t*-test was utilized to compare the numerical data differences between the two groups. Using a one-way analysis of variance (ANOVA) and a Bonferroni *post hoc* correction, differences between several groups were compared. At $P < 0.05$, statistical significance was established.

3. Results

3.1. Brucine suppressed GC cell proliferation and migration

AGS and MKN45 cells were treated with varying amounts of brucine in order to investigate the impact of this drug on the growth of GC cells. The CCK-8 experiment demonstrated that brucine reduced AGS and MKN45 cell viability in a way that depends on the dose (Fig. 2A and B). The IC50 values for AGS and MKN45 cells were 15.45 and 8.76 μM, respectively (Fig. 2A and B). According to our findings, brucine had no effect on the GES-1 cells' ability to survive (Fig. 2C). Thus, brucine did not cause severe damage to normal

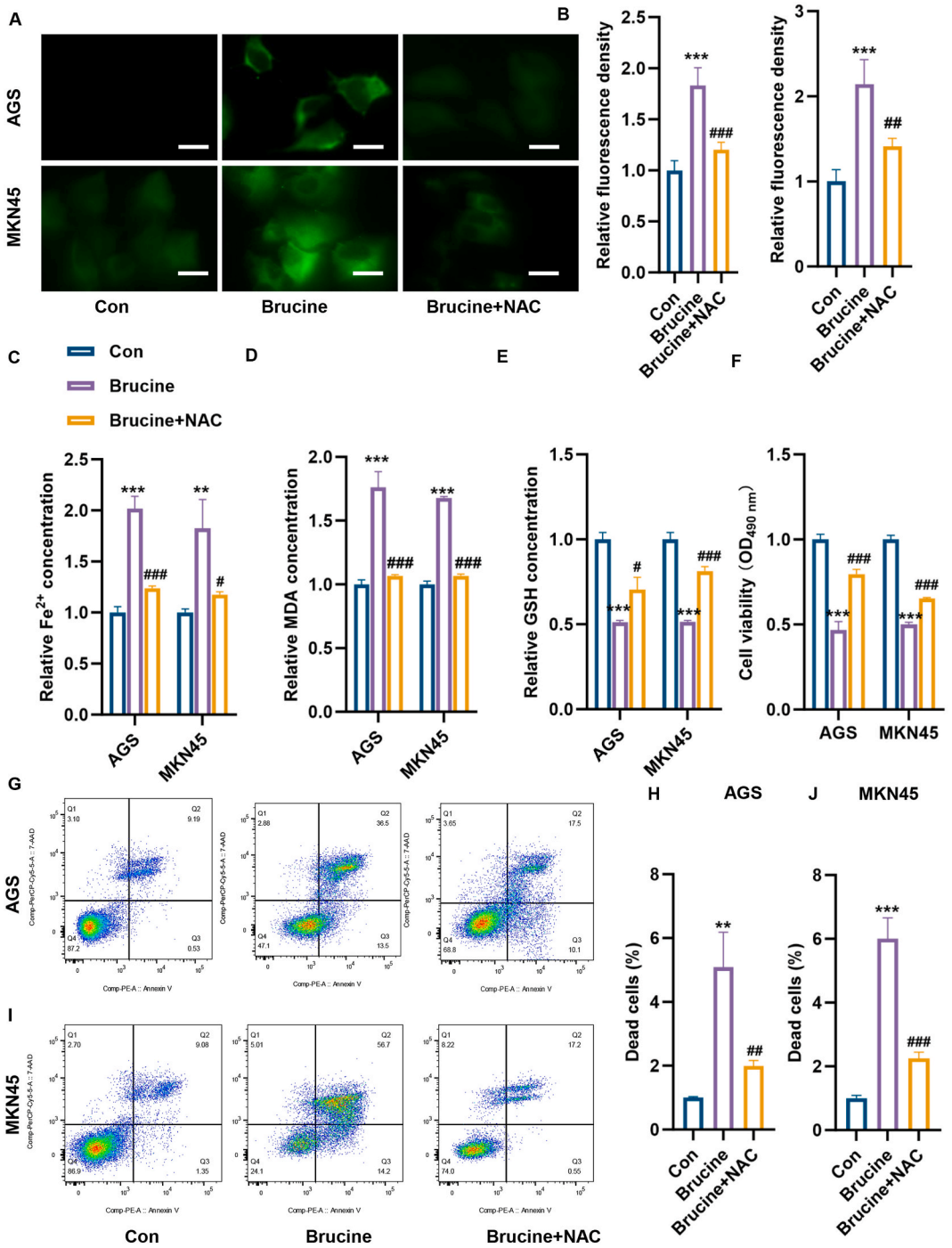

Fig. 4. NAC inhibited brucine-induced lipid peroxidation and cytotoxicity in GC cells. (A) The C11 BODIPY fluorescent probe was used to detect the fluorescence intensity in AGS and MKN45 cells exposed to brucine with or without NAC pretreatment (magnification, 20 × ; scale bar, 10 μm). (B) Statistical analysis of relative fluorescence intensity. Quantification of Fe^{2+} (C), MDA (D), and GSH (E) levels in AGS and MKN45 cells exposed to brucine with or without NAC pretreatment. (F) CCK-8 assays showed that the reduction in cell death induced by brucine can be significantly reversed by NAC in AGS and MKN45 cells. In addition, flow cytometry assays showed that brucine-induced cell death can be partially reversed by preincubation with NAC in AGS (G) and MKN45 (I) cells. Statistical analysis of AGS (H) and MKN45 (J) cell death. n = three independent replicates for each individual experiment. ***p < 0.001 vs. con; ##p < 0.01, ###p < 0.001 vs. brucine.

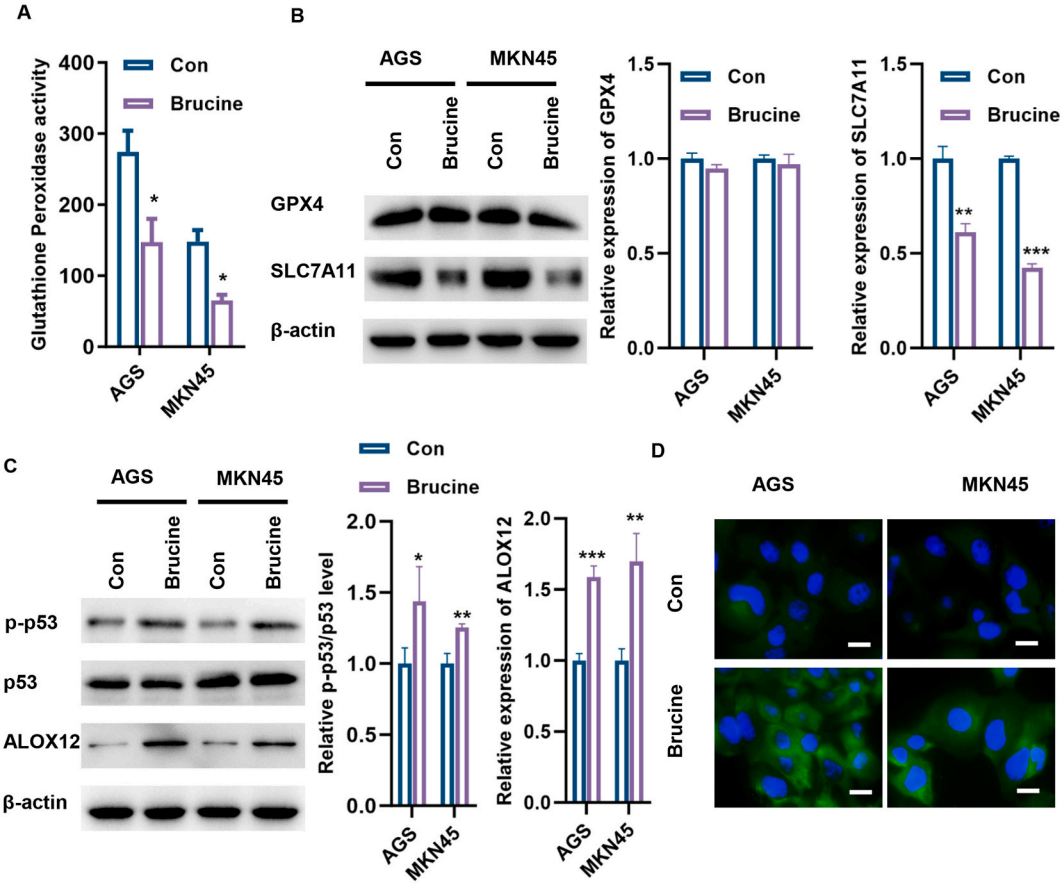

Fig. 5. Brucine enhanced p53 expression and suppressed SLC7A11 expression in GC cells. (A) Brucine decreased glutathione peroxidase activity in AGS and MKN45 cells. (B) Brucine exposure reduced SLC7A11 expression but did not change GPX4 expression in AGS or MKN45 cells. (C) Western blot analysis showing that brucine enhanced p53 and ALOX12 expression in AGS and MKN45 cells. (D) IF staining showing that brucine upregulated p53 expression in AGS and MKN45 cells (magnification, 20 × ; scale bar, 10 μm). n = three independent replicates for each individual experiment. *p < 0.05, **p < 0.01, ***p < 0.001 vs. con.

cells. Transwell assays showed that, compared to the control treatment, brucine treatment significantly suppressed the migration and invasion of AGS and MKN45 cells (Fig. 2D and E). Furthermore, exposure to brucine lowered the rate at which AGS and MKN45 cells healed their wounds in comparison to the control treatment (Fig. 2F and G). These observations indicated the anti-proliferative role of brucine in GC cells.

3.2. *Brucine contributed to ferroptosis in GC cells*

AGS and MKN45 cells were pre-incubated with a pan-caspase inhibitor (z-VAD-FMK), necrosis inhibitor (Ner-1), ferroptosis inhibitor (Fer-1), or autophagy inhibitor (3-MA) in order to investigate the kind of cell death caused by brucine. Compared to the control, Fer-1 significantly protected GC cells from brucine-induced cell death (Fig. 3A and B). We quantified intracellular lipid peroxidation, an important contributor to ferroptosis, in brucine-treated AGS and MKN45 cells with or without Fer-1. As seen in Fig. 3C, pre-incubation with Fer-1 attenuated the effects of brucine exposure on the relative fluorescence intensity in AGS and MKN45 cells. These data demonstrated that brucine causes GC cells to undergo ferroptosis.

3.3. *NAC inhibited brucine-induced lipid peroxidation and cytotoxicity in GC cells*

To validate the function of ROS in ferroptosis caused by brucine, we suppressed the production of lipid peroxidation products using NAC, an ROS scavenger. Brucine increased lipid peroxidation, whereas NAC treatment significantly suppressed lipid peroxidation in AGS and MKN45 cells (Fig. 4A and B). Moreover, brucine induced Fe2+ and MDA production in GC cells but suppressed GSH levels in GC cells (Fig. 4C, D, and E). In contrast, pre-incubation with NAC raised GSH levels and lowered Fe2+ and MDA levels in AGS and MKN45 cells (Fig. 4C, D, and E). The CCK-8 experiment demonstrated that the brucine-induced reduction in cell mortality was significantly reversed by NAC treatment in AGS and MKN45 cells (Fig. 4F). Moreover, brucine-induced cell death was partially

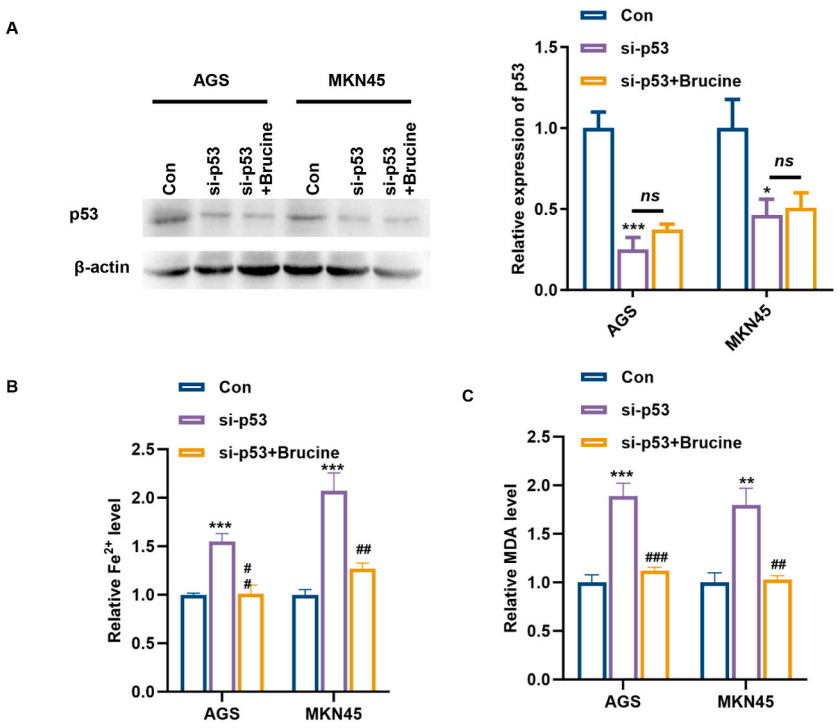

Fig. 6. Brucine-induced ferroptosis was blocked by silencing p53 in GC cells. (A) Western blot assays showed that p53 expression was significantly suppressed in AGS and MKN45 cells treated with or without brucine. p53 knockdown rescued the brucine-induced increase in Fe^{2+} (B) and MDA (C) levels in AGS and MKN45 cells treated with brucine. n = three independent replicates for each individual experiment. ***p < 0.001 vs. con; ##p < 0.01, ###p < 0.001 vs. brucine.

reversed by pre-incubation of AGS and MKN45 cells with NAC (Fig. 4G, H, I, and J).

3.4. Brucine elevated p53 expression and suppressed SLC7A11 expression in GC cells

In order to investigate the fundamental mechanism by which brucine causes GC cells to undergo ferroptosis, we detected glutathione peroxidase activity. Our data showed that brucine treatment decreased glutathione peroxidase activity in AGS and MKN45 cells (Fig. 5A). Interestingly, GPX4 expression was not altered by brucine treatment in GC cells (Fig. 5B). Brucine exposure, however, decreased the expression of SLC7A11 in MKN45 and AGS cells (Fig. 5B). A previous study showed that p53 promotes ferroptosis by suppressing SLC7A11 and activating arachidonate 12-lipoxygenase 12S type (ALOX12) in human tumors [10]. Therefore, we looked into how brucine affected the expression of p53. The findings demonstrated that brucine increased the phosphorylation and p53 and the expression of ALOX12 in AGS and MKN45 cells (Fig. 5C), which are essential for ferroptosis mediated by p53 in response to ROS stress [11]. The increase of p53 in brucine-treated AGS and MKN45 cells relative to the control was also confirmed by IF experiments (Fig. 5D). These data suggest that in AGS and MKN45 cells, brucine causes p53-mediated ferroptosis.

3.5. Brucine-induced ferroptosis can be blocked by silencing p53 in GC cells

To explore whether the induction of autophagy by brucine was due to the activation of p53, a specific siRNA targeting p53 was transfected into AGS and MKN45 cells. The findings demonstrated that, in AGS and MKN45 cells treated with or without brucine, the amount of p53 was significantly suppressed (Fig. 6A). We also evaluated the Fe2+ and MDA concentrations in AGS and MKN45 cells. The brucine-induced elevations in Fe2+ and MDA levels in AGS and MKN45 cells were reversed by p53 knockdown (Fig. 6B and C). Collectively, these data suggest that brucine promotes ferroptosis by increasing p53 expression in GC cells.

3.6. Brucine inhibited the growth of tumors in vivo

We used a xenograft model to determine the pathological role of brucine in cancer. We found that brucine significantly suppressed tumor volume and weight (Fig. 7A, B, and C). Moreover, brucine increased intracellular Fe2+ and MDA levels in tumor tissues (Fig. 7D and E). Western blotting and IHC staining confirmed the in vitro results, brucine significantly increased p53 phosphorylation and expression in tumor tissues in relation to the control (Fig. 7F). Moreover, a significant reduction in SLC7A11 expression was detected in tumor tissues treated with brucine, whereas a significant upregulation of ALOX12 was detected in tumor tissues after brucine

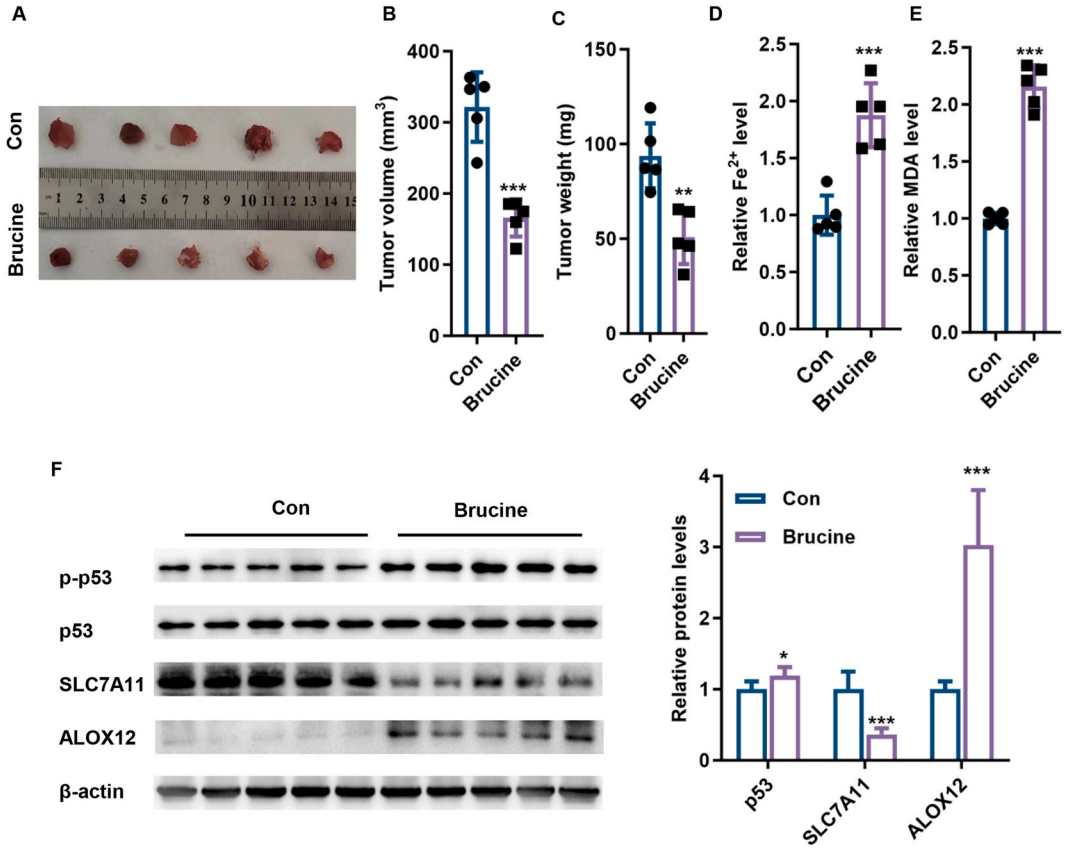

Fig. 7. Brucine suppressed in vivo tumor growth. (A) Representative tumor tissue images. Determination of tumor volume (B) and weight (C). Quantification of intracellular Fe^{2+} (D) and MDA (E) levels in tumor tissues treated with brucine. (F) Western blot analysis showing that brucine increased p53 and ALOX12 expression but decreased SLC7A11 expression. n = five mice in each group. **p < 0.01, ***p < 0.001 vs. con.

treatment (Fig. 7F).

4. Discussion

Currently, surgical resection remains the primary treatment for GC; however, the associated recurrence and metastasis pose significant threats to patient survival [21,22]. Within this context, ferroptosis—a form of oxidative stress that is dependent on iron-dependent, has been identified as critical in antimigratory therapy [23,24]. Notably, in a mouse model of ascite-derived tumors, brucine inhibits tumor growth by attenuating intratumoral angiogenesis and inflammatory responses [25]. Zhao et al. found that brucecine can suppress the proliferation of the transplanted human gastric cancer cell line SGC-7901 and mitigate weight loss in nude mice [26]. Furthermore, in rats with ethanol-induced gastric ulcers, brucine demonstrated therapeutic efficacy acknowledging its antioxidant and anti-inflammatory properties [27]. The remarkable therapeutic potential of brucine in gastrointestinal illnesses is highlighted by these collective studies. Nonetheless, further comprehension of the exact molecular pathways underpinning brucine's anticancer actions on GC is necessary.

In this experiment, the result demonstrated the anti-proliferative impact of brucine on GC cells. Brucine reduced AGS and MKN45 cell viability in a dose- and time-dependent manner, according to the CCK-8 assay. Moreover, in both AGS and MKN45 cells, brucine markedly induced cell death and suppressed their migratory capacity. According to the existing database, this is the first study demonstrating how brucine inhibits GC cells' migration ability.

The experiment further explored the kind of GC cell death caused by brucine. As an inhibitor of ferroptosis, Fer-1 dramatically reversed the cell death caused by brucine, compared to other inhibitors. Therefore, it was inferred from the experimental results that iron mutation is a major factor in the induction of GC cells by Brucine. Moreover, brucine-induced lipid peroxidation was blocked by pre-incubation with Fer-1. Also brucine-induced elevations in MDA, Fe2+, and ROS levels in GC cells were dramatically reversed by NAC, a lipid peroxidation inhibitor. The brucine-mediated inhibition of other tumors has been extensively studied. For example, brucine induces prostate cancer cells to undergo apoptosis via heat shock protein 70 (HSP70) [28]. In cervical cancer, brucine induces apoptosis, attenuates inflammation, and slows the growth of cells by inhibiting PI3K/AKT/mTOR signaling [13]. Through the inhibition of angiogenesis, brucine reduced the malignant proliferation and migration of tumor cells in the triple-negative breast cancer

cell line MDA-MB-231 [29]. These findings imply that brucine inhibits the formation and progression of different tumors through various signal transduction pathways. In contrast, we obtained novel data indicating that brucine suppresses GC by inducing ferroptosis.

Tumor suppressor p53 is involved in various cellular stressors in response to DNA damage, hypoxia, and nutrient starvation [30]. p53 activation induced by high levels of stress or injury may lead to apoptosis and cell death [31]. p53-induced ferroptosis was first reported in 2015 [10]. In a previous study, the authors showed that p53 contributes to ferroptosis in different cancer cells via the transcriptional suppression of SLC7A11 expression without affecting GPX4 expression [10]. According to our research, brucine elevated p53 expression in both MKN45 and AGS cells. In comparison, brucine suppressed the expression of SLC7A11 in GC cells; however, no changes in GPX4 expression were observed. Interestingly, we determined that the GPx activity decreased following brucine treatment. GPX can destroy peroxides and plays a key role in controlling the antioxidant defense system, of which GPX4 is a key component [32,33]. Whether brucine reduces glutathione peroxidase activity without decreasing GPX4 expression remains unknown. We propose that by inhibiting SLC7A11 expression, the brucine-induced increase in p53 expression decreases cysteine uptake, which limits the production of intracellular GSH, a major cellular antioxidant required to maintain glutathione peroxidase activity.

SLC7A11 and SLC3A2 are components of the amino acid transporter System Xc [34]. Moreover, p53 can affect the function of system Xc-by acting on the promoter region of SLC7A11 and negatively affecting its transcription [10,34]. System Xc-is in control of the acquisition of cysteine from the extracellular environment, which is subsequently converted into cysteine in the cytoplasm and subsequently used for GSH synthesis [35,36]. When p53 downregulates SLC7A11, it releases ALOX12, which oxidises the polyunsaturated fatty acid chains of cell membrane phospholipids, generating lipid peroxides [11]. Overabundance of lipid peroxide is the primary risk factor for ferroptosis. In agreement with this, we showed that brucine increased ALOX12 expression, elevated lipid ROS levels, and induced ferroptosis in GC cells.

To verify whether brucine-induced cell death is primarily caused by p53-mediated ferroptosis, siRNA targeting p53 was used to suppress p53-dependent ferroptosis. As mitochondria are major sources of cellular intracellular ROS and changes in mitochondrial morphology are key features of ferroptosis [37], TEM analysis was performed to assess the ultrastructural alterations in the mitochondria of GC cells. The experiment showed that brucine-induced mitochondrial dysfunction was reversed by p53 knockdown. In addition, the results of in vivo experiments showed that brucine treatment reduced tumour weight and volume, and decreased MDA and Fe2+ levels. Meanwhile, Western blotting showed that brucine treatment decreased the expression of SLC7A11, but also increased the expression of p53 and ALOX12. p53 is subject to different post-translational regulatory mechanisms, including phosphorylation, when cells encounter different stimuli. This result shows the diverse functions [38]. When cells are under stress, p53 gets phosphorylated quickly [39]. In this investigation, brucine raised MDA levels, accelerated the deposition of lipid ROS, and decreased GSH levels, suggesting that brucine induces oxidative damage. Based on these results, it can be hypothesised that p53 is phosphorylated in response to oxidative stress and is involved in Brucella-mediated iron apoptosis in GC cells. Blocking cystine uptake leads to a reduction in GSH and GPX4 levels [40,41]. However, brucine did not affect GPX4 expression but suppressed glutathione peroxidase activity. Glutathione peroxidase activity involves the viability of glutathione peroxidases (GPXs)1–4 and includes GPX4 [42–44]. Furthermore, a reduction in GSH levels leads to a decrease in GPX1 and GPX2 expression [42–44]. Interestingly, GPX4, GPX1, and GPX2 are also involved in ferroptosis [42–44]. Accordingly, we hypothesize that although GPX4 expression remains unchanged, there may be other GPXs with altered expression. These findings indicate that brucine-induced ferroptosis is primarily mediated through the p53/SLC7A11/ALOX12 signaling pathway.

This study had several limitations. First, the evidence presented in the current study lacks the time-dose dependence of brucine and ferroptosis. In the future, we plan to measure changes in ferroptosis-related mRNA or protein levels in AGS and MKN45 cells at 12, 24, 48, and 72 h following treatment. Second, both AGS and MKN45 cells will be gastric adenocarcinoma cells. Therefore, it is not possible to determine whether brucine has similar effects in all types of GC or only in adenocarcinoma cells. Third, whether there are potential side effects that limit further exploration or extensive clinical use of these materials should be addressed in future studies. Fourth, there are numerous reports regarding the effects of brucine on cancers such as cervical cancer and glioma [13,15]. However, to yet, no clinical trials have been carried out to examine the impact of brucine on pre- or post-surgical advanced or incipient cancers. In this work, we confirmed that brucine caused ferroptosis, which prevented GC cells from proliferating and migrating. We propose that the clinical application of brucine still has a long way to go. Fourth, it would be interesting to explore whether p53 phospho-mimics can function in the absence of brucine. Future research will assess how p53 p-mimic affects MDA levels and GPX4 activity. Finally, we fully understand how additional mechanistic exploration experiments could further enhance the quality of our paper. However, owing to time and resource constraints, conducting these experiments is beyond the scope of the current research. Future investigations will concentrate on delving further into these important systems.

However, the toxicity of brucine poses a significant challenge to its clinical utility. Even at therapeutic doses, the toxicity of brucine may reach potentially harmful levels, necessitating extreme caution in its therapeutic application to prevent adverse reactions from overdosing [45]. In addition, strychnine, an alkaloid derived from the same plant, is 10–20-fold more toxic than brucine [45]. Irrespective the 98 % purity of brucine, the possibility of contamination with chemicals such as strychnine raises concerns regarding its safety for therapeutic use. Thus, further rigorous assessment of the purity and potential contamination of brucine is crucial to ensure its safety and efficacy in therapeutic applications.

5. Conclusion

Collectively, the current study's findings show that brucine is a strong inducer of ferroptosis in GC cells and that these effects are achieved through p53/SLC7A11/ALOX12 signaling (Fig. 8). The current findings lend support to the idea of using brucine to treat of

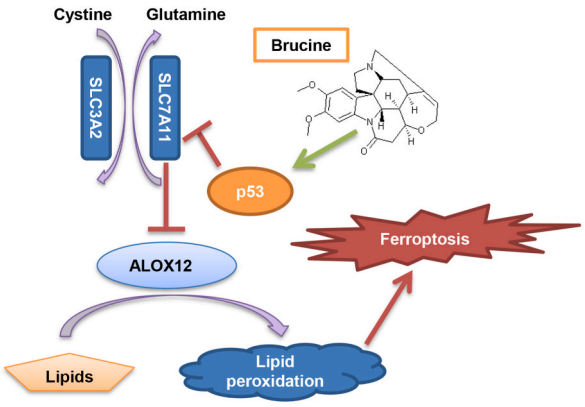

Fig. 8. Graphical summary of the underlying mechanism through which brucine induces ferroptosis in gastric cancer.

GC.

Funding

This study was supported by grants from the Talent Initiation Fund (TIF) of Fengxin County People's Hospital (FX-2021J86).

Ethics approval

This study involving animal subjects was reviewed and approved by the Fengxin County People's Hospital (approval number: 20231252). The work described was performed in accordance with the U.K. Animals (Scientific Procedures) Act, 1986 and associated guidelines, the European Communities Council Directive 2010/63/EU, and the National Institutes of Health Office of Laboratory Animal Welfare policies and laws. This study complied with the ARRIVE guidelines for reporting experiments involving animals. All experiments were conducted in accordance with relevant guidelines and regulations.

Data availability statement

The datasets generated and/or analyzed during the current study are not publicly available due to the inclusion of sensitive data which is protected under privacy regulations. However, data are available from the corresponding author on reasonable request.

CRediT authorship contribution statement

Jincheng Zhai: Writing – review & editing, Writing – original draft, Visualization, Validation, Supervision, Software, Resources, Project administration, Methodology, Investigation, Funding acquisition, Formal analysis, Data curation, Conceptualization. **Jiaxing Min:** Writing – original draft, Visualization, Methodology. **Mingqiang Gong:** Writing – original draft, Visualization, Methodology.

Declaration of competing interest

The authors declare that they have no known competing financial interests or personal relationships that could have appeared to influence the work reported in this paper.

Appendix A. Supplementary data

Supplementary data to this article can be found online at https://doi.org/10.1016/j.heliyon.2024.e33674.

References

[1] F.M. Johnston, M. Beckman, Updates on management of gastric cancer, Curr. Oncol. Rep. 21 (2019) 67.
[2] Z. Guan, J. Chen, X. Li, N. Dong, Tanshinone IIA induces ferroptosis in gastric cancer cells through p53-mediated SLC7A11 down-regulation, Biosci. Rep. 40 (2020).
[3] D. D'Ugo, A. Agnes, M. Grieco, A. Biondi, R. Persiani, Global updates in the treatment of gastric cancer: a systematic review. Part 2: perioperative management, multimodal therapies, new technologies, standardization of the surgical treatment and educational aspects, Updates Surg 72 (2020) 355–378.
[4] T. Irino, S. Matsuda, N. Wada, H. Kawakubo, Y. Kitagawa, Essential updates 2019/2020: perioperative and surgical management of gastric cancer, Ann Gastroenterol Surg 5 (2021) 162–172.

[5] X. Song, X. Wang, Z. Liu, Z. Yu, Role of GPX4-mediated ferroptosis in the sensitivity of triple negative breast cancer cells to gefitinib, Front. Oncol. 10 (2020) 597434.
[6] H. Luo, R. Zhang, Icariin enhances cell survival in lipopolysaccharide-induced synoviocytes by suppressing ferroptosis via the Xc-/GPX4 axis, Exp. Ther. Med. 21 (2021) 72.
[7] J. Liu, R. Kang, D. Tang, Signaling pathways and defense mechanisms of ferroptosis, FEBS J. 289 (2022) 7038–7050.
[8] Y. Wang, M. Zhang, R. Bi, Y. Su, F. Quan, Y. Lin, C. Yue, X. Cui, Q. Zhao, S. Liu, Y. Yang, D. Zhang, Q. Cao, X. Gao, ACSL4 deficiency confers protection against ferroptosis-mediated acute kidney injury, Redox Biol. 51 (2022) 102262.
[9] S. Doll, B. Proneth, Y.Y. Tyurina, E. Panzilius, S. Kobayashi, I. Ingold, M. Irmler, J. Beckers, M. Aichler, A. Walch, H. Prokisch, D. Trumbach, G. Mao, F. Qu, H. Bayir, J. Fullekrug, C.H. Scheel, W. Wurst, J.A. Schick, V.E. Kagan, J.P. Angeli, M. Conrad, ACSL4 dictates ferroptosis sensitivity by shaping cellular lipid composition, Nat. Chem. Biol. 13 (2017) 91–98.
[10] L. Jiang, N. Kon, T. Li, S.J. Wang, T. Su, H. Hibshoosh, R. Baer, W. Gu, Ferroptosis as a p53-mediated activity during tumour suppression, Nature 520 (2015) 57–62.
[11] B. Chu, N. Kon, D. Chen, T. Li, T. Liu, L. Jiang, S. Song, O. Tavana, W. Gu, ALOX12 is required for p53-mediated tumour suppression through a distinct ferroptosis pathway, Nat. Cell Biol. 21 (2019) 579–591.
[12] L. Lu, R. Huang, Y. Wu, J.M. Jin, H.Z. Chen, L.J. Zhang, X. Luan, Brucine, A review of phytochemistry, pharmacology, and toxicology, Front. Pharmacol. 11 (2020) 377.
[13] V.D. Seshadri, Brucine promotes apoptosis in cervical cancer cells (ME-180) via suppression of inflammation and cell proliferation by regulating PI3K/AKT/mTOR signaling pathway, Environ. Toxicol. 36 (2021) 1841–1847.
[14] N. Ishimwe, P. Wei, M. Wang, H. Zhang, L. Wang, M. Jing, L. Wen, Y. Zhang, Autophagy impairment through lysosome dysfunction by brucine induces immunogenic cell death (ICD), Am. J. Chin. Med. 48 (2020) 1915–1940.
[15] S. Lu, X.Z. Wang, C. He, L. Wang, S.P. Liang, C.C. Wang, C. Li, T.F. Luo, C.S. Feng, Z.C. Wang, G.F. Chi, P.F. Ge, ATF3 contributes to brucine-triggered glioma cell ferroptosis via promotion of hydrogen peroxide and iron, Acta Pharmacol. Sin. 42 (2021) 1690–1702.
[16] W. Chen, P. Zou, Z. Zhao, X. Chen, X. Fan, R. Vinothkumar, R. Cui, F. Wu, Q. Zhang, G. Liang, J. Ji, Synergistic antitumor activity of rapamycin and EF24 via increasing ROS for the treatment of gastric cancer, Redox Biol. 10 (2016) 78–89.
[17] J. Wang, L. Zeng, N. Wu, Y. Liang, J. Jin, M. Fan, X. Lai, Z.S. Chen, Y. Pan, F. Zeng, F. Deng, Inhibition of phosphoglycerate dehydrogenase induces ferroptosis and overcomes enzalutamide resistance in castration-resistant prostate cancer cells, Drug Resist. Updates 70 (2023) 100985.
[18] L. Xiong, J. Zhang, H. Shi, G. Zhu, X. Ji, M. Li, P. Zhu, K. Luo, Downregulation of TNFAIP1 alleviates OGD/R-induced neuronal damage by suppressing Nrf2/GPX4-mediated ferroptosis, Exp. Ther. Med. 25 (2023) 25.
[19] A. Ismaeel, J.A. Laudato, E. Fletcher, E. Papoutsi, A. Tice, L.S. Hwa, D. Miserlis, A.Z. Jamurtas, J. Steiner, P. Koutakis, High-fat diet augments the effect of alcohol on skeletal muscle mitochondrial dysfunction in mice, Nutrients 14 (2022).
[20] J.A. Kopechek, C.F. McTiernan, X. Chen, J. Zhu, M. Mburu, R. Feroze, D.A. Whitehurst, L. Lavery, J. Cyriac, F.S. Villanueva, Ultrasound and microbubble-targeted delivery of a microRNA inhibitor to the heart suppresses cardiac hypertrophy and preserves cardiac function, Theranostics 9 (2019) 7088–7098.
[21] Q. Zhao, L. Cao, L. Guan, L. Bie, S. Wang, B. Xie, X. Chen, X. Shen, F. Cao, Immunotherapy for gastric cancer: dilemmas and prospect, Brief Funct Genomics 18 (2019) 107–112.
[22] W. Feng, Y. Ding, W. Zong, S. Ju, Non-coding RNAs in regulating gastric cancer metastasis, Clin. Chim. Acta 496 (2019) 125–133.
[23] F. Ursini, M. Maiorino, Lipid peroxidation and ferroptosis: the role of GSH and GPx4, Free Radic. Biol. Med. 152 (2020) 175–185.
[24] P. Koppula, L. Zhuang, B. Gan, Cystine transporter SLC7A11/xCT in cancer: ferroptosis, nutrient dependency, and cancer therapy, Protein Cell 12 (2021) 599–620.
[25] S.S. Agrawal, S. Saraswati, R. Mathur, M. Pandey, Cytotoxic and antitumor effects of brucine on Ehrlich ascites tumor and human cancer cell line, Life Sci. 89 (2011) 147–158.
[26] L. Zhao, Y. Liu, H. Xu, Inhibitory effect of brucine on SGC-7901 nude mice xenograft model, Chin. J. Cancer Prev. Treat. 19 (2012) 1464–1466.
[27] M. Noman, N.G. Qazi, N.U. Rehman, A.U. Khan, Pharmacological investigation of brucine anti-ulcer potential, Front. Pharmacol. 13 (2022) 886433.
[28] W. Yan, Z. Zeng, F. Qin, J. Xu, Z. Liao, M. Ouyang, Effects of brucine on mitochondrial apoptosis and expression of HSP70 in prostate cancer cells, Transl. Cancer Res. 11 (2022) 500–507.
[29] M.R. Xu, P.F. Wei, M.Z. Suo, Y. Hu, W. Ding, L. Su, Y.D. Zhu, W.J. Song, G.H. Tang, M. Zhang, P. Li, Brucine suppresses vasculogenic mimicry in human triple-negative breast cancer cell line MDA-MB-231, BioMed Res. Int. 2019 (2019) 6543230.
[30] C. Dai, X. Chen, J. Li, P. Comish, R. Kang, D. Tang, Transcription factors in ferroptotic cell death, Cancer Gene Ther. 27 (2020) 645–656.
[31] J. Liu, C. Zhang, J. Wang, W. Hu, Z. Feng, The regulation of ferroptosis by tumor suppressor p53 and its pathway, Int. J. Mol. Sci. 21 (2020).
[32] Y. Miao, Y. Chen, F. Xue, K. Liu, B. Zhu, J. Gao, J. Yin, C. Zhang, G. Li, Contribution of ferroptosis and GPX4's dual functions to osteoarthritis progression, EBioMedicine 76 (2022) 103847.
[33] S. Ma, L. Sun, W. Wu, J. Wu, Z. Sun, J. Ren, USP22 protects against myocardial ischemia-reperfusion injury via the SIRT1-p53/slc7a11-dependent inhibition of ferroptosis-induced cardiomyocyte death, Front. Physiol. 11 (2020) 551318.
[34] C. Zeng, J. Lin, K. Zhang, H. Ou, K. Shen, Q. Liu, Z. Wei, X. Dong, X. Zeng, L. Zeng, W. Wang, J. Yao, SHARPIN promotes cell proliferation of cholangiocarcinoma and inhibits ferroptosis via p53/SLC7A11/GPX4 signaling, Cancer Sci. 113 (2022) 3766–3775.
[35] R. Kang, G. Kroemer, D. Tang, The tumor suppressor protein p53 and the ferroptosis network, Free Radic. Biol. Med. 133 (2019) 162–168.
[36] T. Hong, G. Lei, X. Chen, H. Li, X. Zhang, N. Wu, Y. Zhao, Y. Zhang, J. Wang, PARP inhibition promotes ferroptosis via repressing SLC7A11 and synergizes with ferroptosis inducers in BRCA-proficient ovarian cancer, Redox Biol. 42 (2021) 101928.
[37] G. Ye, Z. Xie, H. Zeng, P. Wang, J. Li, G. Zheng, S. Wang, Q. Cao, M. Li, W. Liu, S. Cen, Z. Li, Y. Wu, Z. Ye, H. Shen, Oxidative stress-mediated mitochondrial dysfunction facilitates mesenchymal stem cell senescence in ankylosing spondylitis, Cell Death Dis. 11 (2020) 775.
[38] Q. Chen, Y. Wu, Z. Dai, Z. Zhang, X. Yang, Phosphorylation and specific DNA improved the incorporation ability of p53 into functional condensates, Int. J. Biol. Macromol. 230 (2023) 123221.
[39] N.J. MacLaine, T.R. Hupp, How phosphorylation controls p53, Cell Cycle 10 (2011) 916–921.
[40] Angeli J.P. Friedmann, M. Schneider, B. Proneth, Y.Y. Tyurina, V.A. Tyurin, V.J. Hammond, N. Herbach, M. Aichler, A. Walch, E. Eggenhofer, D. Basavarajappa, O. Radmark, S. Kobayashi, T. Seibt, H. Beck, F. Neff, I. Esposito, R. Wanke, H. Forster, O. Yefremova, M. Heinrichmeyer, G.W. Bornkamm, E.K. Geissler, S. B. Thomas, B.R. Stockwell, V.B. O'Donnell, V.E. Kagan, J.A. Schick, M. Conrad, Inactivation of the ferroptosis regulator Gpx4 triggers acute renal failure in mice, Nat. Cell Biol. 16 (2014) 1180–1191.
[41] T.M. Seibt, B. Proneth, M. Conrad, Role of GPX4 in ferroptosis and its pharmacological implication, Free Radic. Biol. Med. 133 (2019) 144–152.
[42] R. Wei, H. Qiu, J. Xu, J. Mo, Y. Liu, Y. Gui, G. Huang, S. Zhang, H. Yao, X. Huang, Z. Gan, Expression and prognostic potential of GPX1 in human cancers based on data mining, Ann. Transl. Med. 8 (2020) 124.
[43] H. Huang, Y. Dai, Y. Duan, Z. Yuan, Y. Li, M. Zhang, W. Zhu, H. Yu, W. Zhong, S. Feng, Effective prediction of potential ferroptosis critical genes in clinical colorectal cancer, Front. Oncol. 12 (2022) 1033044.
[44] M. Yu, J. Liu, L. Li, H. Xu, Y. Xing, Y. Zhao, Z. Yu, Pharmacokinetic parameters of three active ingredients hederacoside C, hederacoside D, and a-hederin in Hedera helix in rats, J. Separ. Sci. 39 (2016) 3292–3301.
[45] B. Achappa, D. Madi, Y.P. Babu, S. Mahalingam, Rituals can kill - a fatal case of brucine poisoning, Australas. Med. J. 5 (2012) 421–423.